EasyChair Preprint

№ 8437

Topologies of Shear and Strain Promote Chaotic Mixing in Helical Flow

Priyam Chakraborty

July 10, 2022

Topologies of shear and strain promote chaotic mixing in helical flow

Priyam Chakraborty

Happymonk AI Labs, Karnataka, 560078, India
priyam@happymonk.co

Abstract. Physics aids explainable artificial intelligence. The inherent topology of a chaotic system is often a boon to learning algorithms. Helical or screw flows are chaotic. Their velocity and rotational fields are parallel to each other, typically hosting coherent structures that contain (either strain or shear) barriers which resist fluid flow across them. Here, we apply perturbation to coherent fluid particles to construct a criterion governing the topological changes in their mixing across barriers, which we define using the macroscopic statistical measure of finite-time Lyapunov exponent. Our findings demonstrate that the rigid coherent structures essentially support mixing in purely helical flows. These findings have far-reaching implications in diverse fields of applications, ranging from dynamos in growing magnetic field, classical turbulence in superfluid helium to supercell atmospheric tornadoes.

Keywords: chaos, helicity, Lyapunov exponent, streamline

1 Introduction

The topology of chaotic signals around equilibria is an active area of interest in data-centric computing and neural networks. A chaotic signal is deterministic and bounded while being sensitive to initial conditions. Chaotic signals have been recently represented as artificial neurons in the novel ChaosNet architecture to improvise machine-enabled classification [1]. To add, asymptotic perturbations have defined constriction factors which ensure the diversity of solutions in multi-objective optimizations in learning algorithms [2]. Recent studies have affirmed that the Langevin [3] and Lagrangian [4] approaches unravel the underlying physics of neural networks in data science. Since the application of machine learning is gaining traction to comprehend the physics of fluid flow [5], the topological examination of a certain flow field is the subject matter of this article.

Helicity is a flow property which measures the extent of alignment between a vector and its curl. Kinetic helicity quantifies that alignment between vorticity (rotationality) and velocity in the flow. Rotating column of fluid mass in tornado may be an ideal use case of purely helical flow. By virtue of conservation [6, 7], helicity is a fundamental quantity in explaining the dynamo which is a spontaneously growing magnetic field in an electrically conducting Earth's liquid

core [8, 9]. This has interdisciplinary implications, ranging from examining the astrophysical magnetism to assessing the stability of magnetic field in thermonuclear fusion [10]. It is known that a geometrically constrained advection of helical flow hosting a repeated sequence of stretch, twist and fold can be described by a superposition of three orthogonal components of velocity also known as ABC flow, which is attributed to the contributions by Arnol'd, Beltrami and Childress [11]. ABC flow is an exact solution to the steady Euler equations of motion. The modeled flow comprises compartments or cells due to the alternate presence of saddles and foci which is evident from the application of critical point theory [12]. The cells may be associated with rigid coherent structures which modulate fluidic mixing. Rigidity is a measure of increase in timescale of coherence in the mixing phenomenon. An ideal rigid coherent structure neither grows nor decays with time.

Fluidic mixing in purely helical flows is an outstanding area of interdisciplinary interest. Chaotic advection facilitates mixing which in turn depends on repelling stationary points [8]. ABC flow is elusively simple but the pathlines stretch and fold owing to bounded helicity and space-periodicity [13]. Recently, we have examined the topology and transport of mixing in ABC flows using the instantaneous and Lagrangian descriptors [14]. The physical connection between the time-resolved (Eulerian) and time-averaged (Lagrangian) description of mixing in helical flow is the subject matter of this article.

Here, we claim that a topological change in fluid mass that is advecting between locally minimized shear and strain in rigid coherent structures promotes mixing in purely helical unsteady flow. In order to test the hypothesis, we examine the topology of unsteady streamlines and find an asymptotic match between material curves that satisfies smooth mixing under constrained shear and strain. The assessment begins with velocity. Taking cue from the earlier works [15, 16] on unsteady helical rotationalities, a kinematic template of velocity (u, w) in the incompressible helical (ABC) flow may be given as:

$$\begin{aligned} u &= A\,\sin(k(z+\sin(A\,t/\lambda_{ABC}))) + C_0\,\cos(k(y+\sin(A\,t/\lambda_{ABC}))) \\ w &= C_0\,\sin(k(y+\sin(A\,t/\lambda_{ABC}))) + B_0\,\cos(k(x+\sin(A\,t/\lambda_{ABC}))) \end{aligned} \tag{1}$$

where the unsteady parameter A is given as $A_0 + 0.5 \times t \times \sin(\pi\,t)$, t denotes time, the constant parameters A_0, B_0 and C_0 obey the constraint $A_0^2+B_0^2+C_0^2 = 3$, $k = 2\pi/\lambda_{ABC}$ and λ_{ABC} is the length scale of the domain. The flow field in Eq. 1 has dimensions in SI. For illustrations in this article, $A_0 = B_0 = \sqrt{3/2}$, $C_0 = 0$ and $\lambda_{ABC} = 1$.

The significance of the present work is that it unifies the underlying mixing due to helical rotationalities in apparently distinct physical systems, such as the Earth's magnetic dynamo, superfluid helium and tornado. A dynamo comprises the nonlinear interactions between the chaotic flow and the magnetic field within the Earth's liquid core [10]. Chaos modulates the separation of nearby fluid parcels which is often measured with the finite-time Lyapunov exponent (FTLE) that has interdisciplinary applications. For instance, the Lyapunov exponent is frequently used to diagnose nonlinear signals from the human brain

[17]. Alexakis [18], in his search for sustained growing dynamos, computed FTLE in laminar ABC flow and reported certain intervals of the model parameters A, B and C that define chaos. However, this finding alone does not adequately explain the underlying mixing, as attributable to a recent study by the present authors that deliberates the topology of mixing in generalized helical flows by using FTLE in the coordinate space rather than the parametric space of the model [14]. Chaotic motions are essential elements of fast dynamos, i.e., dynamos that operate over timescales much shorter than the turnover timescales generating the fluid flow. Within the Earth's liquid core, a relaxing magnetic field is topologically equivalent to a state of magnetostatic equilibrium which is analogous to Euler flow. Core flow, being turbulent, is asymmetric (that is, chiral with non-zero helicity) [10]. This allows for solving the magnetic field with a tractable idealized ABC flow. In the study of turbulence in superfluid helium, ^{4}He II, Angstrom(Å)-thick superfluid vortex lines have been modeled [19], their existence and growth within normal fluid vortex cores have been quantified [20], and the mechanisms of superfluid – normal fluid vortex matching have been identified [16]. It is well-known that discrete turbulent normal fluid vortices are ideally analogous to those appearing in ABC flow, subject to the condition that the turbulent vortices in ^{4}He II are not closely spaced to initiate any topological change or reconnection [21]. From a geophysical view, the study of tornadoes is crucial to the climatic modeling of the Earth's heat imbalance [22]. Supercell storms originate near swirling intersection of warm inflow and cool outflow. Strong wind shear around bulk updraft orients the vortical flow to be optimally helical in order for the storm to be a sustainable tornado [23]. Which supercell storm transforms into tornado is an open problem [24]. This article complements the progress in these challenges.

Rest of the article is organized as follows. We examine the instantaneous flow topology and identify characteristic timescales in the modeled flow. We probe the topology using Lagrangian descriptors such as pathlines and FTLE to emphasize the fundamental differences between steady and unsteady ABC flow. We then perturb the deformation of fluid parcels to identify the conditions of smooth mixing between minimized strain and shear in the flow where FTLE vanishes. These regions are associated with rigid coherent structures and occupy bulk of the flow. Finally, we discuss the implications of our results on interdisciplinary physical systems and conclude this article.

2 Topological regimes in helical flow

We find that the temporal probes of the modeled flow field [Eq. 1] at different locations in the domain [Fig. 1] suggest that the model is bounded which is essential for the representation of physical flows. We now consider the topological evolution of the model to examine the categorically distinct mixing phenomenon of unsteady helical flow. Figure 2 illustrates the topological bifurcations as a function of time in the x–z plane at $y = 0$ where the Cartesian coordinates have their origin at the centre of the plane. To aid the visualization, we superpose

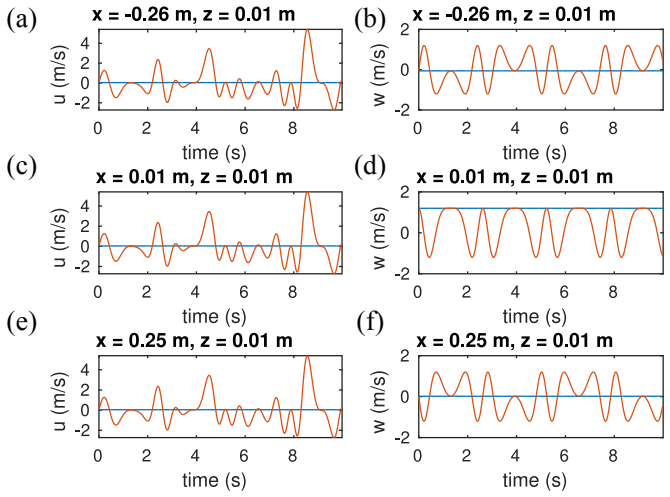

Fig. 1. (a) to (f): Variation of flow components (u, w) with time for steady (horizontal blue) and unsteady (fluctuating red) ABC flow at three specified locations

the streamlines on the vorticity field (ω_y) of ABC flow in Fig. 2. We find three topological regimes where saddles and vortices undergo unique deformations. First, locally maximum vorticity traces the domain of the unsteady flow with time ($t < 1.15\,s$, $1.5\,s < t < 3.25\,s$, $3.27\,s < t < 3.62\,s$ and $4.2\,s < t < 5\,s$). Please see Figs. 2(a), 2(b) and 2(c) for illustration. This is reported in the context of superfluid turbulence as well [16]. Second, there are two occurrences of abrupt topological bifurcation, $3.25\,s < t < 3.27\,s$ [Figs. 2(d), 2(e), 2(f)] and $3.77\,s < t < 3.79\,s$. The bifurcations are evident from the evolving pattern of streamlines. Third, there are regions of vorticity which evolve and grow while being stationary on certain time intervals ($1.15\,s < t < 1.5\,s$, $3.62\,s < t < 3.77\,s$ and $3.79\,s < t < 4.2\,s$). Please see Figs. 2(g), 2(h) and 2(i) for illustration. Thus, the repeated sequence of the three regimes is a candidate that facilitates mixing.

Probing further, we examine the continuum deformation that is associated with flow topology. Two neutrally buoyant neighboring fluid particles separate exponentially over time as elucidated by a first-order Taylor series expansion of the velocity field about a spatial coordinate. This leads to computing the growth rate of a multi-dimensional neighborhood. Consider a two-dimensional flow map $F : (\bar{x}_0, t_0) \rightarrow (\bar{x}, t)$. Initial neighborhood $\delta(\bar{x}_0)$ acted upon by the deformation operator $\bar{\nabla}F$ results in $\delta(\bar{x}) = (\bar{\nabla}\mathrm{F})\,\delta(\bar{x}_0)$. Hence $|\delta(\bar{x})|^2 = \langle(\bar{\nabla}F)\,\delta(\bar{x}_0), (\bar{\nabla}F)\,\delta(\bar{x}_0)\rangle = \langle\delta(\bar{x}_0), (\bar{\nabla}F)^T\bar{\nabla}F\,\delta(\bar{x}_0)\rangle = \langle\delta(\bar{x}_0), C\,\delta(\bar{x}_0)\rangle$. Here $\langle .,. \rangle$ denotes inner product and C is the Cauchy-Green strain tensor, which is positive-definite. Accordingly, all its eigenvalues ($\lambda_i, i = 1, 2, 3$) are positive. Mass conservation between instants t_0 and t for an incompressible flow requires

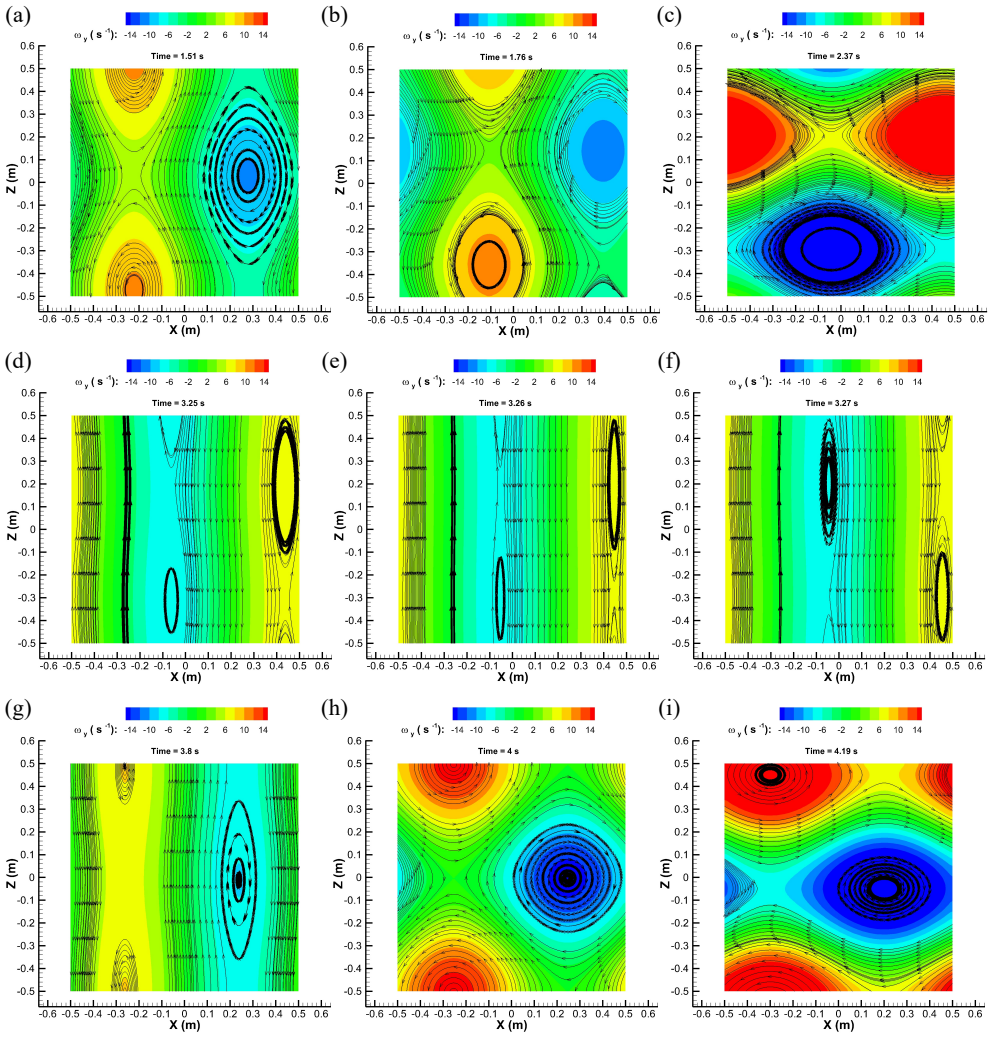

Fig. 2. Topological regimes in unsteady ABC flow. The vorticity field (ω_y) and the interplay of superimposed streamlines suggest that there are three distinct topological regimes: (a) to (c), (d) to (f) and (g) to (i). The illustrative streamlines are equal in number from (a) to (i).

the determinant of C to be unity (§14 of Lamb 25). This implies that, in two dimensions (2D), $\lambda_1 \times \lambda_2 = 1$, that is, λ_1 and λ_2 must satisfy the inequality: $0 < \lambda_1 \leq 1 \leq \lambda_2$ [26]. We note that, since the stretch, twist and fold of vortices in helical systems do not constitute the subject matter of this article, there is no loss of generality in examining a 2D modeled ABC flow. The 2D velocity field (u, w) exhibits chaos the way it exists in a three-dimensional system [27]. Moreover, the imposed length scale in the third dimension is far greater than the mixing scale of the helicity-driven dynamics. For instance, the size of the Earth and troposphere are orders of magnitude larger than the cross-sections of the Earth's liquid core and tornado, respectively. Thus, a 2D model enables a conservative understanding of mixing.

The extent of deformation of an n-dimensional fluid mass may be defined in terms of n Lyapunov exponents along principal directions which are given by the eigenvectors of the tensor C. Since the separation of neighbors in the flow is exponential, the largest Lyapunov exponent overwhelms the remaining $(n-1)$ exponents. Mathematically, the time-averaged logarithmic largest Lyapunov exponent is known as FTLE, that is, FTLE $= \frac{1}{\Delta t}\log(\lambda_n)$. Thus, the fluid particles attract and repel along λ_1 and λ_2, respectively, in 2D flow. When the eigenvalues of C are each unity, FTLE is zero which implies coherence due to no net exponential growth or decay. Starting with the velocity of the modeled ABC flow [Eq. 1], we computed FTLEs that denote the repulsion of fluid parcels from these structures forward in time. We sampled the model at every 0.01 second for 1000 time steps and customized an open-source software for the computations. We employed a fourth-order Runge-Kutta scheme to discretize time.

3 Perturbation of coherent fluid parcels

To elucidate the topological changes in coherent structures as shown in Fig. 2, we may quantify the deformation of a neutrally buoyant material curve in the flow [Fig. 3]. Mathematically, a length-averaged property $Q(\gamma) = \frac{1}{\sigma}\int_0^\sigma \mathcal{L}(\bar{r}(s), \bar{r}'(s))ds$ of curve γ in ϵ-neighborhood is invariant with $O(\epsilon^2)$-accuracy if the differential of Q vanishes (that is, when Q is indifferent to change in γ). Here, s denotes the length along γ. $\bar{r}$ is a position on γ and $\bar{r}'$ is the tangent to γ at that point [Fig. 3]. Minimizing Q gives a set of Euler equations subject to which the total derivative of a function (known as the first integral) vanishes when $\mathcal{L}$ is independent of s (see supplementary material). The first integral is invariant for the curve γ which is traveling with the flow given that the Q-minimizing condition is true (known as Noether's theorem) [28].

Physically, Q may be constructed to imply that either strain or shear governs the flow. Firstly, when Q is defined as a strain ratio (l_t/l_0) by comparing the parametric lengths of curve γ at a later and initial time instants, the dimensional scaling of s with respect to $\bar{r}'$ transforms $\mathcal{L}$ to $\mathcal{L}'(\bar{r}, \bar{r}') = \langle \bar{r}', \frac{1}{2}(C - \lambda^2 I)\bar{r}' \rangle$, which is a function of strain energy (Supplementary material of Haller and Beron-Vera 29) and defines an energy integral. The tensor $\frac{1}{2}(C - \lambda^2 I)$ in 2D flow has oppositely signed eigenvalues $\lambda_1 - \lambda^2$ and $\lambda_2 - \lambda^2$, and is known as a symmetric

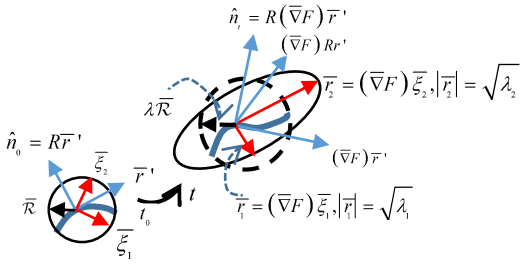

Fig. 3. Deformation of a material curve (solid blue) and the vectors attached to it. $\bar{\xi}_1$, $\bar{\xi}_2$ comprise principal directions in an illustrative 2D deformation.

Lorentzian metric in the geometric sense. The net deformation due to the tensor has two components: isotropic due to λ, and anisotropic due to λ_1 and λ_2 [Fig. 3]. The energy integral ensures a minimum-strain deformation of curve γ in the Lorentzian metric space which confirms that FTLE vanishes at least once within a coherent vortical region enclosed by curve γ in the flow [29]. The vanishing FTLE is a fundamental observation in the analysis of ABC flow presented in this article [Fig. 4].

Secondly, when Q is defined as a shear due to the projection of the advected unit normal vector on the tangent vector, $\mathcal{L}$ transforms into a new $\mathcal{L}'$ which contains $\frac{1}{2}(CR-RC)$ that is again a symmetric Lorentzian metric tensor because its eigenvalues in 2D, $\pm\sqrt{C_{12}^2 + \frac{(C_{22}-C_{11})^2}{4}}$, have opposite sign. Accordingly, the energy integral ensures a minimum-shear deformation of curve γ. Here, $C = \begin{bmatrix} C_{11} & C_{12} \\ C_{12} & C_{22} \end{bmatrix}$, and $R = \begin{bmatrix} 0 & -1 \\ 1 & 0 \end{bmatrix}$ rotates a vector counter-clockwise by $\frac{\pi}{2}$.

Figure 4 shows that the coherent FTLEs divide the domain into 'cells'. Moreover, we attribute mixing to the sensitive pathlines of fluid particles which are spread over greater parts of the domain in the unsteady modeled flow than in the steady flow. To this end, we have shown earlier that the transport in generalized helical flows is a function of topology and FTLE [14]. Here, we examine the conditions which underlie the topological differences during the transport of a material curve through shear- and strain-driven cells of the domain under the influence of vanishing FTLE. Since the definition of the length-averaged property Q minimizes either strain or shear of a deforming curve γ, it is incumbent that there are separate corresponding geometric descriptions of the phenomena. Accordingly, a tangent $\bar{r}'$ to a point on the closed material curve γ that is advecting in the flow with a minimum-strain deformation may be given as [26]:

$$\bar{r}'(s) = \frac{\sqrt{\lambda_2 - \lambda^2}}{\sqrt{\lambda_2 - \lambda_1}}\bar{\xi}_1(\bar{r}) \pm \frac{\sqrt{\lambda^2 - \lambda_1}}{\sqrt{\lambda_2 - \lambda_1}}\bar{\xi}_2(\bar{r}) \tag{2}$$

which is a linear combination of orthonormal eigenvectors, $\bar{\xi}_1$ and $\bar{\xi}_2$, of the tensor C. Similarly, $\bar{r}'$ for a curve γ under minimum shear may be given as [30]:

$$\bar{r}'(s) = \frac{\sqrt{\sqrt{\lambda_2}}}{\sqrt{\sqrt{\lambda_1}+\sqrt{\lambda_2}}}\bar{\xi_1}(\bar{r}) \pm \frac{\sqrt{\sqrt{\lambda_1}}}{\sqrt{\sqrt{\lambda_1}+\sqrt{\lambda_2}}}\bar{\xi_2}(\bar{r}) \tag{3}$$

Since the transition of the curve γ from a minimizing strain to shear deformation requires that the Eqs. 2 and 3 are linearly dependent, the corresponding coefficients of $\bar{\xi_1}$ and $\bar{\xi_2}$ in these two equations must be proportional to each other. Since the eigenvalues λ_1 and λ_2 of the tensor C approach unity when FTLE is vanishing, Eqs. 2 and 3 have characteristic differences. While the coefficient of either $\bar{\xi_1}$ or $\bar{\xi_2}$ is $\frac{1}{\sqrt{2}}$ in Eq. 3, we consider an asymptotic perturbation to avoid singularity in Eq. 2. Noting that $\lambda_2 = 1/\lambda_1$, we let $\epsilon = \sqrt{1-\lambda_1^2}$ to be the perturbation when λ_1 approaches unity. As $\epsilon \to 0$, a transition between shear- and strain-minimizing curves in the flow will occur when there is asymptotic matching between Eqs. 2 and 3 with respect to the coefficients of $\bar{\xi_1}$ and $\bar{\xi_2}$.

After some algebra, the matching between the coefficients of $\bar{\xi_1}$ occurs according to:

$$\tfrac{1}{\epsilon}\sqrt{1-\lambda^2\sqrt{1-\epsilon^2}} \sim \tfrac{1}{\sqrt{2}} \tag{4}$$

which implies that $1-\lambda^2(1-\frac{\epsilon^2}{2}-\frac{\epsilon^4}{8}) \sim \frac{\epsilon^2}{2}$, and hence $\lambda \to 1^+$. Similarly, the coefficients of $\bar{\xi_2}$ match when:

$$\tfrac{1}{\epsilon}\sqrt{\lambda^2\sqrt{1-\epsilon^2}-(1-\epsilon^2)} \sim \tfrac{1}{\sqrt{2}} \tag{5}$$

which leads to $\lambda^2 \sim \frac{1-\frac{\epsilon^2}{2}}{\sqrt{1-\epsilon^2}}$, and hence $\lambda \to 1^+$. That is, λ is never less than one. Thus, we find that the presence of rigid coherent structures (λ on the order of but not less than one) is a necessary condition for the characteristic topological modulations in unsteady helical ABC flow.

4 Discussion

Our findings have implications on the study of terrestrial magnetic dynamos, superfluid turbulence and tornadoes. First, the equation of magnetic induction may be expressed as $\partial\bar{B}/\partial t = \bar{\nabla}\times(\bar{u}\times\bar{B}) + (\nabla^2\bar{B})/R_m$, where $\bar{u}$ and $\bar{B}$ are velocity and magnetic fields respectively, and $R_m = U_c L_c \mu_0 \sigma$ is non-dimensional magnetic Reynolds number with U_c and L_c being characteristic velocity and length respectively, μ_0 being free space permeability and σ being electrical conductivity. Solution to the induction equation reveals the largest Lyapunov exponent (indicator of chaos) and unstable critical points, both of which can be used as metrics to find a relation that tweaks the parameters A, B and C of the unsteady ABC flow with varying R_m (and hence U_c and L_c) so that FTLE contours can bear equivalent metrics. Actual solutions of induction equation with ABC velocity field at lower values of R_m are required to establish this relation. This can provide apriori information about advection of magnetic field when R_m is high ($O(\sim 10^3)$ for Earth) and direct solution of the induction equation is delayed due

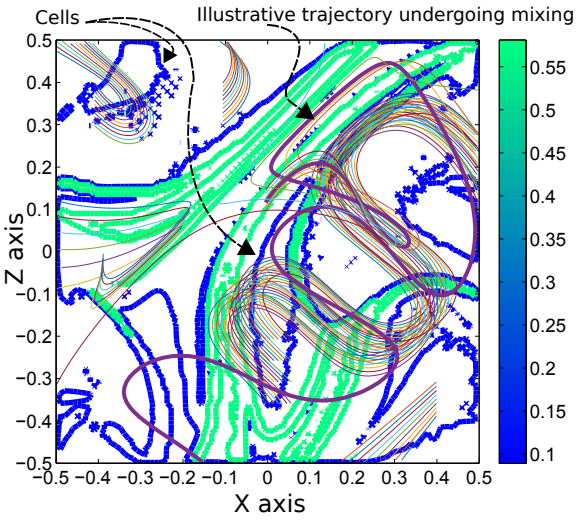

(a)

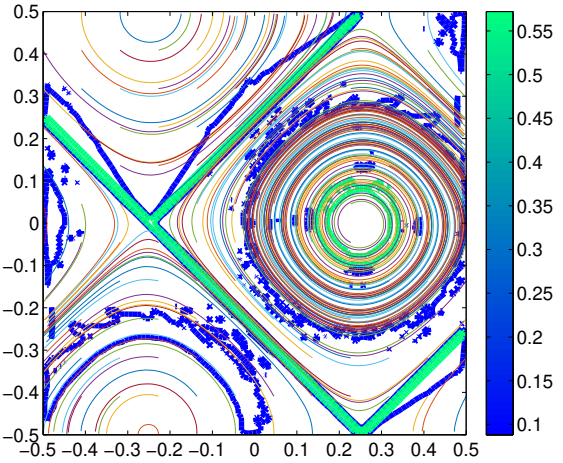

(b)

Fig. 4. Forward FTLE Contour superimposed with trajectories. (a) unsteady ABC flow, (b) steady ABC flow

to constraint on computing power. Moreover, unsteady ABC flow shows promise in being used as input to induction equation to find growth rates of both large scale and small scale dynamos over a wide range of R_m [31]. We do realize that anti-dynamo theorem [32] negates formation of sustained growing dynamo in 2D flow. However, our analysis in this article can be easily extended and is applicable to three dimensions. Second, particle image velocimetry and direct numerical solution of the equation of moving particles in fluid are potent tools for flow visualization of He II. However, they depend on properties of particles being injected as tracers [33]. FTLE contour of ABC flow displays presence of idealized discrete vortices of superfluid He II without requiring tracers. Instantaneous maximum vorticity regions in our unsteady model are found to linearly trace the domain as has been reported with other unsteady models [16]. Onset of vortex wave instability as mechanism for superfluid – normal fluid vortex matching [16] can be linked with FTLE contours. Moreover, there is scope to explore analogy between cell mixing in unsteady ABC flow and turbulent vortex interactions in superfluid He II at temperatures varying below critical $2.17K$. Third, observations from Doppler Radar [34] can be used to identify unsteady ABC flow field with matched critical stagnation points. This is to be followed by tagging the supercell storms, both objectively (largest FTLE) and subjectively (extent of cell mixing due to zero-level FTLE contours). Thus storm tagging will help build a database documenting the behavior of storms leading to tornadoes.

5 Conclusion

To summarize, we analyze the significance of macroscopic Lagrangian behavior and mixing characteristics of purely helical flow in understanding the first principles of interdisciplinary problems. In this regard, we consider an unsteady model of helical flow, and identify coherent structures in both steady and unsteady helical flow. Fluid mixing across cells is absent in the steady but evident in the unsteady flow. We identify distinct topological changes in the unsteady flow as well. These observations highlight the role of perturbation in unsteady field and affirms our new analytical procedure to understand how coherent fluid parcels transition between shear and strain barriers and hence induce cell mixing. Largest FTLE in the domain and the degree of cell mixing appear to emerge as two indicators that extend the scope of purely helical flow as a model for dynamo theory, mixing in superfluid He II and tagging of supercell tornadoes.

Acknowledgments

The author is grateful to Professor Snehanshu Saha (CSIS and APPCAIR, BITS Pilani, K. K. Birla Goa Campus, Goa, India) for his insightful comments and review of the manuscript.

Bibliography

[1] Balakrishnan HN, Kathpalia A, Saha S, Nagaraj N (2019) ChaosNet: A chaos based artificial neural network architecture for classification. Chaos: An Interdisciplinary Journal of Nonlinear Science 29(11):113,125

[2] Bhattacharya A, Saha S, Nagaraj N (2021) SMPSO revisited : A theoretical analysis of exponentially-averaged momentum in multi-objective problems. DOI 10.48550/ARXIV.2104.10040, URL https://arxiv.org/abs/2104.10040

[3] Marceau-Caron G, Ollivier Y (2017) Natural langevin dynamics for neural networks. In: International Conference on Geometric Science of Information, Springer, pp 451–459

[4] Cranmer M, Greydanus S, Hoyer S, Battaglia P, Spergel D, Ho S (2020) Lagrangian neural networks. arXiv preprint arXiv:200304630

[5] Vinuesa R, Brunton SL (2022) Enhancing computational fluid dynamics with machine learning. Nature Computational Science 2(6):358–366

[6] Enciso A, Peralta-Salas D, Torres de Lizaur F (2016) Helicity is the only integral invariant of volume-preserving transformations. Proc Natl Acad Sci USA 113(8):2035–2040, DOI 10.1073/pnas.1516213113, URL http://www.pnas.org/lookup/doi/10.1073/pnas.1516213113, 1602.04745

[7] Scheeler MW, Kleckner D, Proment D, Kindlmann GL, Irvine WTM (2014) Helicity conservation by flow across scales in reconnecting vortex links and knots. Proc Natl Acad Sci USA 111(43):15,350–15,355, DOI 10.1073/pnas.1407232111

[8] Moffatt HK (1989) Stretch, twist and fold. Nature 341:285–286, DOI 10.1038/340301a0, nature.vol.342.30nov1989

[9] Gilbert AD (1991) Fast dynamo action in a steady chaotic flow. Nature 350:483–485, DOI 10.1038/353737a0

[10] Moffatt HK (2014) Helicity and singular structures in fluid dynamics. Proc Natl Acad Sci USA 111(10):3663–3670, DOI 10.1073/pnas.1400277111, URL http://www.pnas.org/cgi/doi/10.1073/pnas.1400277111

[11] Dombre T, Frisch U, Greene JM, Henon M, Mehr A, Soward AM (1986) Chaotic streamlines in the ABC flows. J Fluid Mech 167:353–391

[12] Strogatz SH (1994) Nonlinear Dynamics and Chaos with applications to physics, biology, chemistry, and engineering. Perseus Books

[13] Ottino J (1990) Mixing, chaotic advection, and turbulence. Annu Rev Fluid Mech 22(1):207–253, DOI 10.1146/annurev.fluid.22.1.207, URL http://fluid.annualreviews.org/cgi/doi/10.1146/annurev.fluid.22.1.207

[14] Chakraborty P, Roy A, Chakraborty S (2021) Topology and transport in generalized helical flows. Physics of Fluids 33(11):117,106

[15] Haller G (2001) Distinguished material surfaces and coherent structures in three-dimensional fluid flows. Physica D 149(4):248–277, DOI 10.1016/S0167-2789(00)00199-8

[16] Barenghi CF, Samuels DC, Bauer GH, Donnelly RJ (1997) Superfluid vortex lines in a model of turbulent flow. Phys Fluids 9(9):2631–2643, DOI 10.1063/1.869379

[17] Mohanchandra K, Saha S, Murthy KS (2016) Evidence of chaos in EEG signals: An application to BCI. In: Advances in Chaos Theory and Intelligent Control, Springer, pp 609–625
[18] Alexakis A (2011) Searching for the fastest dynamo: Laminar ABC flows. Phys Rev E 84(2):026,321(10), DOI 10.1103/PhysRevE.84.026321, 1105.3692
[19] Schwarz KW (1982) Generation of superfluid turbulence deduced from simple dynamical rules. Phys Rev Lett 49(4):283–285, DOI 10.1103/PhysRevLett.59.2117
[20] Samuels DC (1993) Response of superfluid vortex filaments to concentrated normal-fluid vorticity. Phys Rev B 47(2):1107–1110
[21] Paoletti MS, Fisher ME, Sreenivasan KR, Lathrop DP (2008) Velocity statistics distinguish quantum turbulence from classical turbulence. Phys Rev Lett 101(15):154,501(4), DOI 10.1103/PhysRevLett.101.154501, 0808.1103
[22] Diffenbaugh NS, Scherer M, Trapp RJ (2013) Robust increases in severe thunderstorm environments in response to greenhouse forcing. Proc Natl Acad Sci USA 110(41):16,361–16,366, DOI 10.1073/pnas.1307758110, URL http://www.pnas.org/cgi/doi/10.1073/pnas.1307758110
[23] Lilly DK (1986) The structure, energetics and propagation of rotating convective storms. Part II: helicity and storm stabilization. DOI 10.1175/1520-0469(1986)043⟨0126:TSEAPO⟩2.0.CO;2
[24] Rotunno R (2013) The Fluid Dynamics of Tornadoes. Annu Rev Fluid Mech 45(1):59–84, DOI 10.1146/annurev-fluid-011212-140639, URL http://www.annualreviews.org/doi/10.1146/annurev-fluid-011212-140639
[25] Lamb H (1975) Hydrodynamics. Cambridge University Press
[26] Haller G (2015) Lagrangian coherent structures. Annu Rev Fluid Mech 47:137–162, DOI 10.1146/annurev-fluid-010313-141322
[27] Galloway DJ, Proctor MRE (1992) Numerical calculations of fast dynamos in smooth velocity fields with realistic diffusion. Nature 356:691–693
[28] Gelfand I, Fomin SV (1963) Calculus of variations. Prentice-Hall, Inc.
[29] Haller G, Beron-Vera FJ (2013) Coherent Lagrangian vortices: the black holes of turbulence. J Fluid Mech 731:R4–1 – R4–10, DOI 10.1017/jfm.2013.391, 1308.2352
[30] Haller G, Beron-Vera FJ (2012) Geodesic theory of transport barriers in two-dimensional flows. Physica D 241:1680–1702
[31] Cameron A, Alexakis A (2016) Fate of alpha dynamos at large Rm. Phys Rev Lett 117(20):205,105(5), DOI 10.1103/PhysRevLett.117.205101, 1607.07294
[32] Zil'dovich IB (1957) The magnetic field in the two-dimensional motion of a conducting turbulent liquid. J Exptl Theoret Phys 31:460–462
[33] Poole DR, Barenghi CF, Sergeev YA, Vinen WF (2005) Motion of tracer particles in He II. Phys Rev B 71(6):064,514(16), DOI 10.1103/PhysRevB.71.064514
[34] Wurman J, Straka JM, Rasmussen EN (1996) Fine-Scale Doppler Radar Observations of Tornadoes. Science 272:1774–1777, DOI 10.1126/science.272.5269.1774